J. Fluid Mech. (1988), *vol.* 197, *pp.* 57–79
Printed in Great Britain

Numerical calculations of the primary-flow exchange process in the Taylor problem

By K. A. CLIFFE
Theoretical Physics Division, UKAEA Harwell Laboratory, Didcot, Oxon OX11 0RA, UK

(Received 23 July 1984 and in revised form 6 May 1988)

Numerical methods are used to study the way in which the number of cells present in the Taylor experiment changes as the length of the comparatively short annulus varies. The structure of the solution surface is determined by following paths of singular points in a finite-element discretization of the axisymmetric Navier–Stokes equations. The numerical results are compared with the experiments of Benjamin (1978*b*), Mullin (1982) and Mullin *et al.* (1982). The calculations are in agreement with the qualitative theory of Benjamin (1978*a*) and Schaeffer (1980) except that in the interaction involving four- and six-cell flows, the numerical calculations indicate that the six-cell flow can become unstable owing to perturbations that are antisymmetric about the midplane.

1. Introduction

In this paper we study Taylor–Couette flow in a comparatively short annulus using numerical methods. The inner cylindrical wall rotates and the outer cylinder and both ends are stationary. The principal phenomenon under study is how the number of Taylor vortices present in the *primary flow* changes as the length of the annulus varies. The primary flow may be defined as that produced by slowly increasing the speed of the inner cylinder from rest. It is thus smoothly connected to the uniquely defined flow at low Reynolds number.

This problem appears to have been studied first by Benjamin (1978*a*, *b*). In his apparatus he was able to vary the angular speed, Ω, of the inner cylinder, and the length, l, of the annulus; in any particular experimental run l is fixed and Ω varied. The non-dimensional speed is the Reynolds number defined as $R = \Omega r_1 d/\nu$, where r_1 is the radius of the inner cylinder, $d = r_2 - r_1$ the width of the annulus, r_2 the radius of the outer cylinder and ν the kinematic viscosity of the fluid. The non-dimensional length is the aspect ratio defined as $\Gamma = l/d$. Benjamin's data are shown in figure 1. For aspect ratios less than that corresponding to point C, the primary flow is symmetrical and has two Taylor cells. The cells develop, as R is gradually increased through a narrow range of values, in a continuous manner. The absence of a definite critical value of R for the onset of cells is due to the presence of the ends (Kusnetsov *et al.* 1977; Benjamin & Mullin 1982). For aspect ratios greater than that corresponding to B the primary flow smoothly develops four cells. In the range of aspect ratios between B and C the primary flow first develops a weak four-cell structure but as the line BC is crossed this changes abruptly to a two-cell flow. If the Reynolds number is then reduced, so that DC is crossed, this two-cell flow collapses back to the weak four-cell flow. Thus the experimental observations exhibit a hysteresis phenomenon. Using ideas from elementary catastrophe theory and abstract mathematical results from the theory of the Navier–Stokes equations,

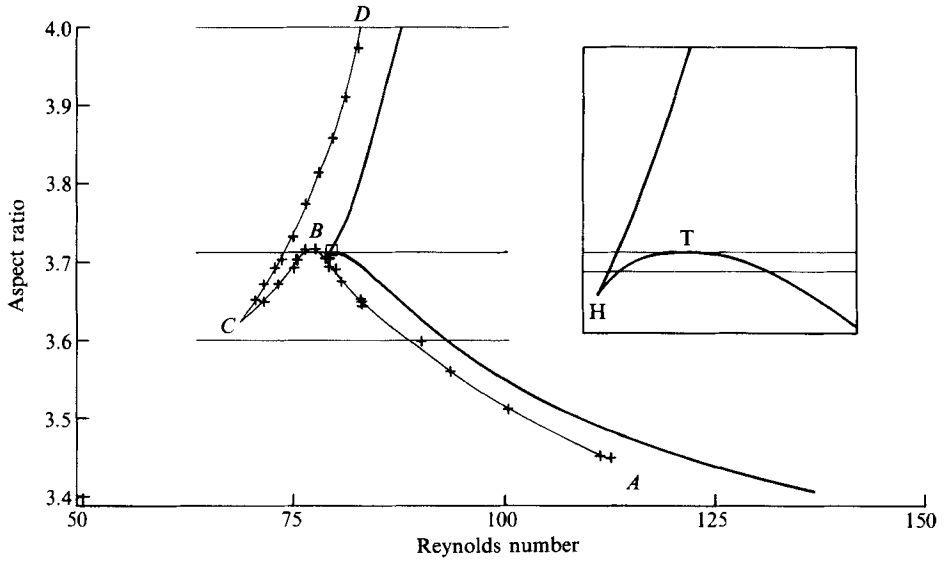

FIGURE 1. Experimentally (+) and numerically (−) determined bifurcation set in the (R, Γ)-plane for two-cell and four-cell flows. Experimental points from Benjamin (1978*b*). An enlargement of the region near the transcritical and hysteresis points is shown in the inset.

Benjamin interpreted his data as follows: at C the primary flow has a non-degenerate hysteresis point so that for aspect ratios greater than C the primary solution branch has an S shape with the middle part representing an unstable steady flow. At B the two-cell and four-cell flows exchange roles as the primary flow through a transcritical bifurcation point. It should be noted that Benjamin's analysis of his experimental data requires very little input from the Navier–Stokes equations. Consequently his theory cannot predict which way the cusp at C points. Indeed, Mullin (1982) found that for the exchange process involving four-cell and six-cell, six cell and eight-cell, and ten-cell and twelve-cell flows the cusp pointed upwards, whereas it pointed downwards for the eight-cell–ten-cell exchange. A similar result, i.e. the cusp pointing upwards, for the four-cell–six-cell exchange was found by Mullin, Pfister & Lorenzen (1982) in an experiment with a smaller radius ratio.

An important qualitative analysis of the effects of the ends of the annulus on the primary-flow exchange process was provided by Schaeffer (1980). He introduced an extra parameter, τ, into the idealized problem, where $0 \leqslant \tau \leqslant 1$. The value of τ determines the boundary conditions imposed on the end faces: $\tau = 0$ corresponds to periodic boundary conditions, whilst $\tau = 1$ corresponds to the physically realistic no-slip boundary conditions. The parameter τ is regarded as a homotopy parameter which interpolates between the two extremes. Schaeffer applied the Lyanpunov–Schmidt procedure to the periodic problem at a value of the aspect ratio such that the two-cell and four-cell modes bifurcate at the same Reynolds number. This leads to a set of two nonlinear equations in two unknowns, which are essentially the amplitudes of the two-cell and four-cell flow. These equations contain certain parameters, which were assumed to satisfy various inequalities. Schaeffer analysed the effects of the ends by applying the methods of singularity theory (Golubitsky & Schaeffer 1979) to determine the possible bifurcation diagrams for small positive values of τ. Schaeffer further argued that since he obtained a definite set of

bifurcation diagrams, the qualitative features of the flow would be similar for small τ and for $\tau = 1$. Indeed Schaeffer's analysis produced precisely the same qualitative effects as had been observed by Benjamin. Schaeffer's analysis is important because it provides a definite link between the Navier–Stokes equations and the type of phenomena observed by Benjamin. Because Schaeffer did not carry out explicit calculations in his Lyanpunov–Schmidt reduction procedure, he was unable to predict the direction in which the cusp points. Further, his analysis, strictly speaking, applies to the exchange process between $2k$ and $2k+2$ cells where $k \geqslant 2$. Thus the case studied by Benjamin is excluded. The reason for this is that Schaeffer's model has cubic nonlinearities, whereas the case $k = 1$ would also involve quadratic terms. However Schaeffer points out (Schaeffer 1980, footnote to p. 313) that, under certain weak conditions, the quadratic terms may not affect the qualitative behaviour of the equations.

Schaeffer's model has been studied, using perturbation methods, by Hall (1980, 1982). The degeneracy that gives rise to the quadratic terms mentioned above prevented Hall from producing results to compare with all Benjamin's data. In particular, he was unable to calculate the phenomenon associated with CD in figure 1, which he suggests may have to be obtained by numerical means. In his second paper Hall (1982) treated the problem of the exchange between the four-cell and six-cell flow. He found that the constants appearing in the Schaeffer model lead to a bifurcation diagram with the cusp pointing upwards, which is consistent with the observations of Mullin (1982). However, the extent of the region over which hysteresis could be observed was much smaller in Hall's calculations than in the experiments. This is perhaps not surprising since the approximations used by Hall are likely to have large errors when the perturbation parameter, τ, is close to 1. Nevertheless, Hall's work is significant in that it is the first attempt to make a quantitative connection between the Navier–Stokes equations and the flows in the Taylor experiment with small aspect ratio.

It is apparent from the above description of previous theoretical work on this problem that the essential difficulty is that the ends of the cylinders always induce an $O(1)$ perturbation of the basic flow. Thus it seems unlikely that perturbation methods will be able to give sufficiently accurate results for a realistic comparison with experiment. A further point to consider is that both Schaeffer and Hall assumed that the modes interacting during the exchange process are all symmetric about the mid-plane of the apparatus; since the flows observed in the primary-flow exchange have this feature the assumption seems reasonable. However, as we show later, in the four–six-cell exchange there is a range of aspect ratio over which the six-cell flow becomes unstable to non-symmetric disturbances; all the non-symmetric solutions are in fact unstable but they do affect indirectly what is observed. Tuckerman (1983) and Schrauf (1986) have shown that symmetry breaking is important in the related spherical Taylor–Couette problem.

In this paper we study the primary-flow exchange process using numerical techniques similar to those used by the author to study two-cell and single-cell flows (Cliffe 1983). The axisymmetric Navier–Stokes equations and appropriate boundary conditions are discretized using the finite-element method to give a finite set of nonlinear equations which depend on three parameters: the Reynolds number, aspect ratio and radius ratio defined by $\eta = r_1/r_2$. Continuation methods and numerical methods for bifurcation problems are then applied to this set of equations. In particular we calculate paths of limit points and symmetry-breaking pitchfork bifurcation points which correspond to the loci of collapse points observed in the

experiments. Certain points on these paths of singular points correspond to more complex singularities (having higher codimension) and we also present calculations of these special points. We have used grids sufficiently fine so that the errors in our calculated critical points are less than 1%. Thus we are able to make a quantitative comparison of the numerical results with the experiments quoted above. The agreement is, on the whole, quite satisfactory. The calculations also reveal that for the four–six exchange the situation is more complex than the Schaeffer model indicates, with asymmetric solutions of the Navier–Stokes equations present. The rest of the paper will be as follows. In §2 we describe the numerical methods used. In §3 the results for the two–four and four–six exchanges are described and compared with the experimental data of Benjamin (1978*b*), Mullin (1982) and Mullin *et al.* (1982). Some conclusions are drawn in §4.

2. Numerical methods

In cylindrical polar coordinates (r^*, ϕ, z^*) with the origin midway between the ends of the annulus, and velocity $\boldsymbol{U}^* \equiv (u_r^*, u_\phi^*, u_z^*)$, the equations for axisymmetric flow of a viscous fluid are

$$R\left(\Gamma u_r \frac{\partial u_r}{\partial r} + u_z \frac{\partial u_r}{\partial z} - \frac{\Gamma u_\phi^2}{(r+\beta)}\right) + \Gamma \frac{\partial p}{\partial r} - \frac{\Gamma}{(r+\beta)} \frac{\partial}{\partial r} 2(r+\beta) \frac{\partial u_r}{\partial r} - \frac{\partial}{\partial z}\left(\frac{1}{\Gamma}\frac{\partial u_r}{\partial z} + \frac{\partial u_z}{\partial r}\right) + \frac{2\Gamma u_r}{(r+\beta)^2} = 0, \quad (2.1)$$

$$R\left(\Gamma u_r \frac{\partial u_\phi}{\partial r} + u_z \frac{\partial u_\phi}{\partial z} + \Gamma \frac{u_r u_\phi}{(r+\beta)}\right) - \frac{\Gamma}{(r+\beta)} \frac{\partial}{\partial r}(r+\beta) \frac{\partial u_\phi}{\partial r} - \frac{1}{\Gamma} \frac{\partial^2 u_\phi}{\partial z^2} + \frac{\Gamma u_\phi}{(r+\beta)^2} = 0, \quad (2.2)$$

$$R\left(\Gamma u_r \frac{\partial u_z}{\partial r} + u_z \frac{\partial u_z}{\partial z}\right) + \frac{\partial p}{\partial z} - \frac{1}{(r+\beta)} \frac{\partial}{\partial r}(r+\beta)\left(\Gamma \frac{\partial u_z}{\partial r} + \frac{\partial u_r}{\partial z}\right) - \frac{2}{\Gamma} \frac{\partial^2 u_z}{\partial z^2} = 0, \quad (2.3)$$

$$\frac{\Gamma}{(r+\beta)} \frac{\partial}{\partial r}(r+\beta) u_r + \frac{\partial u_z}{\partial z} = 0. \quad (2.4)$$

In the above equations r, z, $\boldsymbol{U}$ and p are given by

$$r = \frac{r^*}{d} - \beta, \quad z = \frac{z^*}{l}, \quad \boldsymbol{U} = \frac{\boldsymbol{U}^*}{r_1 \Omega}, \quad p = \frac{dp^*}{\mu r_1 \Omega},$$

where μ is the dynamic viscosity, Ω is the angular speed of the inner cylinder, $d = r_2 - r_1$, $\beta = r_1/d = \eta/(1-\eta)$ and $\eta = r_1/r_2$ is the radius ratio, where r_2 and r_1 are the radii of the outer and inner cylinders respectively. The aspect ratio $\Gamma = l/d$ and the Reynolds number $R = r_1 \Omega d/\nu$, were ν is the kinematic viscosity.

Equations (2.1)–(2.4) hold in the region

$$D = \{(r, z) \mid 0 \leqslant r \leqslant 1, \ -0.5 \leqslant z \leqslant 0.5\}. \quad (2.5)$$

The boundary conditions are that u_r and u_z are zero on the entire boundary of D, and that u_ϕ is zero on the outer cylinder ($r = 1$) and one on the inner cylinder ($r = 0$). On the ends ($z = \pm 0.5$), u_ϕ is zero except near the inner cylinder where it increases smoothly to one over a small distance, ϵ. The exact value of ϵ and the variation of u_ϕ will depend on the details of the experiment; however, we have found the results

to be insensitive to the value of ϵ and therefore conclude that any sufficiently small value will be adequate.

As a starting point for the finite-element discretization, (2.1)–(2.4) are converted into a nonlinear operator equation in an appropriate Hilbert space. When this Hilbert space is replaced by a finite-dimensional (finite-element) subspace the result is a finite-element approximation of (2.1)–(2.4). The mathematical details of this procedure will not be presented here since they are not essential to the present paper and have been covered elsewhere (Cliffe 1983; Cliffe & Spence 1984, 1986). In the method we use, the region D is covered by a mesh of nine-node quadrilateral elements; on each element the components of velocity are approximated by biquadratic polynomials and the pressure is approximated by piecewise linear functions which are not, in general, continuous across element boundaries (Cliffe, Jackson & Greenfield 1982; Engleman *et al.* 1982; Cliffe 1983).

The finite-element equations may be written in the form (Cliffe & Spence 1984, 1986)

$$\boldsymbol{f}(\boldsymbol{x}, R, \Gamma) = \boldsymbol{0}, \quad \boldsymbol{f}: \boldsymbol{X} \times \mathbb{R} \times \mathbb{R} \to \boldsymbol{X}, \tag{2.6}$$

where $\boldsymbol{x}$ is a vector containing all the velocity and pressure degrees of freedom. The space $\boldsymbol{X}$ is the set of all possible $\boldsymbol{x}$ and is equivalent to $\mathbb{R}^N$, where N is the total number of degrees of freedom in the problem. The $\boldsymbol{f}$ in (2.6) has an important symmetry property which reflects the fact that the Navier–Stokes equations are invariant under reflection about the midplane of the annulus. It can be shown (Cliffe & Spence 1984, 1986) that, provided the mesh is symmetric, there exists a linear mapping, S, from $\boldsymbol{X}$ to $\boldsymbol{X}$ such that

$$S \neq I, \quad S^2 = I \quad \text{and} \quad \boldsymbol{f}(S\boldsymbol{x}, R, \Gamma) = S\boldsymbol{f}(\boldsymbol{x}, R, \Gamma) \quad \boldsymbol{x} \in \boldsymbol{X}, \quad R, \Gamma \in \mathbb{R}. \tag{2.7}$$

We used the Keller arclength-continuation method to calculate individual solution branches (Keller 1977). The stability limits of the various flows correspond to either simple limit points or symmetry-breaking bifurcation points. Limit points were calculated by applying Keller arclength continuation to the following system of equations (Moore & Spence 1980; Jepson & Spence 1985):

$$F(\boldsymbol{y}, \Gamma) \equiv \begin{pmatrix} \boldsymbol{f}(\boldsymbol{x}, R, \Gamma) \\ \boldsymbol{f}_{\boldsymbol{x}}(\boldsymbol{x}, R, \Gamma)\boldsymbol{\varphi} \\ \boldsymbol{l}\boldsymbol{\varphi} - 1 \end{pmatrix} = \boldsymbol{0}, \tag{2.8}$$

with $\boldsymbol{y} = (\boldsymbol{x}, \boldsymbol{\varphi}, R)$, $\boldsymbol{\varphi} \in \boldsymbol{X}$ and $\boldsymbol{l} \in \boldsymbol{X}'$ (the dual of $\boldsymbol{X}$).

More degenerate points may be encountered along a path of limit points. In a two-parameter problem there are just two possibilities, namely a non-degenerate hysteresis point (which we denote by H) and a transcritical bifurcation point (which we denote by T). The projection of the path of limit points onto the (R, Γ)-plane has a characteristic cusp shape at H and a turning point at T. Details of the numerical methods used to compute these points may be found in Cliffe & Spence (1986) and Jepson & Spence (1985).

We now consider the implications of the symmetry property (2.7). The mapping S induces a natural decomposition of $\boldsymbol{X}$ into

$$\boldsymbol{X} = \boldsymbol{X}_{\mathrm{s}} + \boldsymbol{X}_{\mathrm{a}}, \tag{2.9}$$

where

$$\boldsymbol{X}_{\mathrm{s}} = \{\boldsymbol{x} \in \boldsymbol{X} \mid S\boldsymbol{x} = \boldsymbol{x}\}, \quad \boldsymbol{X}_{\mathrm{a}} = \{\boldsymbol{x} \in \boldsymbol{X} \mid S\boldsymbol{x} = -\boldsymbol{x}\}, \tag{2.10}$$

consist of the *symmetric* and *antisymmetric* elements of $\boldsymbol{X}$ respectively. Paths of symmetry-breaking bifurcations were calculated by applying Keller arc-length continuation to the following extended system (Werner & Spence 1984):

$$\boldsymbol{F}(\boldsymbol{y},\Gamma)=\left.\begin{pmatrix} \boldsymbol{f}(\boldsymbol{x},R,\Gamma) \\ \boldsymbol{f}_{\boldsymbol{x}}(\boldsymbol{x},R,\Gamma)\boldsymbol{\varphi} \\ \boldsymbol{l}\boldsymbol{\varphi}-1 \end{pmatrix}=\boldsymbol{0},\quad \begin{matrix} \boldsymbol{y}=(\boldsymbol{x},\boldsymbol{\varphi},R)\in\boldsymbol{Y} \\ \boldsymbol{Y}=\boldsymbol{X}_{\mathrm{s}}\times\boldsymbol{X}_{\mathrm{a}}\times\mathbb{R} \\ \boldsymbol{F}\colon \boldsymbol{Y}\times\mathbb{R}\to\boldsymbol{Y} \end{matrix}\right\}. \tag{2.11}$$

It is important to note both the similarity with (2.8) and the essential difference, namely that $\boldsymbol{x}$ must belong to $\boldsymbol{X}_{\mathrm{s}}$ and $\boldsymbol{\varphi}$ must belong to $\boldsymbol{X}_{\mathrm{a}}$. Thus the basic solution is symmetric but the eigenvector is antisymmetric so that the bifurcating branch is asymmetric. The set of points $(\boldsymbol{x},R,\Gamma)$ such that (2.11) is satisfied by $(\boldsymbol{y},\Gamma)$ defines a curve which lies on the symmetric solution surface. This curve is the intersection of the surface of asymmetric solutions with the symmetric ones.

A path of symmetry-breaking bifurcation points may itself have a limit point. Cliffe & Spence (1984) call this type of singularity a coalescence point because two symmetry-breaking bifurcation points coalesce at such a point. There are two types of coalesence point which we denote by C^{+} and C^{-}. At C^{+} an isola of asymmetric solutions is born whereas at C^{-} a pair of asymmetric solution branches intersect on the symmetric solution branch.

Another type of singularity that can occur on a path of symmetry-breaking bifurcation points is a quartic symmetry-breaking bifurcation point, which we denote by Q (Cliffe & Spence 1984). Here the bifurcating asymmetric branch has quartic dependence on the excess Reynolds number near the singularity rather than quadratic dependence. For values of Γ on one side of the singular point the bifurcation is supercritical whereas on the other side it is subcritical. We also note that a pair of paths of limit points on the asymmetric solution surface splits off from the symmetric solution at Q.

The final type of singularity that can occur along a path of symmetry-breaking bifurcation points is called a double singular S-point, which we shall denote by D (Werner 1984). This is a point at which a limit point and symmetry-breaking point coincide.

Details of the numerical methods used to compute the points C, Q and D are given in Cliffe & Spence (1986) and Cliffe, Jepson & Spence (1986). It is also important to note that in calculating symmetry-breaking singular points the symmetry condition can be used to reduce, by approximately half, the number of degrees of freedom in the problem (Cliffe & Spence 1986). This is done, essentially, by discretizing the lower (i.e. $z\leqslant 0$) half of the domain D.

A typical mesh is shown in figure 2. All the meshes used were uniform in the r- and z-directions with the exception of the elements in the corners next to the inner cylinder where local refinement of the type shown in figure 2 was used. The purpose of this refinement was to model the rapid variation in the azimuthal velocity component between the inner cylinder and ends of the cylinder. For calculations of the symmetric flows and for the symmetry-breaking bifurcation points only half of the region D need be discretized (Cliffe & Spence 1986), whereas the full region D must be used for the non-symmetric solutions. The meshes for the full region may be characterized by the triple (NR,NZ,NC), where NR and NZ are the numbers of elements in the r- and z-directions respectively and the mesh has $2NC-1$ elements in each corner. A mesh for half the region D will be denoted by (NR,NZ,NC,S) and is essentially equivalent to that part of a $(NR,2NZ,NC)$ mesh with $z\leqslant 0$. The total

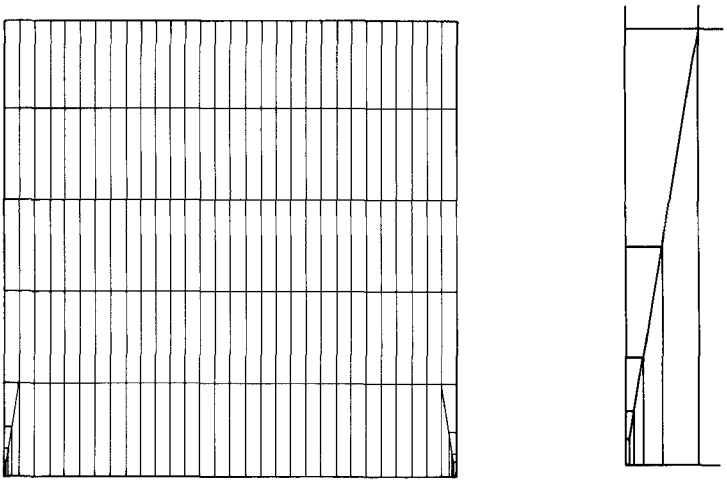

FIGURE 2. A $(5, 30, 5)$ mesh and an enlargement of the local refinement used in the corner.

Mesh	Critical R at aspect ratio 3.4	Critical R at aspect ratio 4
$5, 10, 5, S$	139.71	87.650
$8, 10, 5, S$	138.82	87.571
$10, 20, 5, S$	138.58	87.566
$15, 30, 5, S$	138.41	87.564

TABLE 1. Effect of mesh refinement on the critical Reynolds numbers at the two extremes of the path of limit points for the two–four exchange.

number of degrees of freedom on a (NR, NZ, NC) mesh is $3(2NR+1)(2NZ+1)+60(NC-1)+3NRNZ+12(NC-1)$ and on a (NR, NZ, NC, S) mesh is $3(2NR+1)(2NZ+1)+30(NC-1)+3NRNZ+6(NC-1)$. We found, as previously (Cliffe 1983), that the results were insensitive to the values of NC provided it was greater than about 4. The calculations for the two–four exchange used a $(5, 10, 5, S)$ mesh having 1107 degrees of freedom; and, for the four–six exchange $(5, 15, 5, S)$ and $(5, 30, 5)$ meshes having 1512 and 2991 degrees of freedom respectively. As an exception the path of symmetry-breaking bifurcation points for $\Gamma < 5.0$ was computed using a $(10, 30, 5, S)$ mesh having 5007 degrees of freedom. The results were checked for accuracy by repeating various calculations on a sequence of finer meshes. These mesh refinement calculations were performed at the extremes of the paths of limit points and symmetry-breaking bifurcation points where, because the Reynolds numbers are higher, the discretization errors are expected to be greatest. Refinement checks were also done at the degenerate points H, T, Q, C^+ and C^-.

The results for the extremes of the path of limit points in the two–four exchange are shown in table 1. From them we estimate that the error in the critical Reynolds number using the $(5, 10, 5, S)$ mesh is about 0.1 % at aspect ratio 4 and about 1 % at aspect ratio 3.4. The results of the other checks indicate that the error in the critical Reynolds number along all the computed paths of limit points and symmetry-breaking bifurcation points is at most 1 %. The error in the critical values of Reynolds

number and aspect ratio for the degenerate points is much less than this, typically of order 0.1%.†

As a further check the code was used to calculate the critical Reynolds numbers for the onset of Taylor vortices in the periodic case; the meshes used here gave results that agree with those of Roberts (1965) to 0.5%. On refining the mesh the results converged to Roberts' values.

3. Results

In this section we present the results of our numerical calculations and compare them with the available experimental data. The experiments determined the loci of points in the (R, Γ)-plane which mark the loss of stability of various flows. These loci correspond to paths of singular points as described in the previous section, and the principal comparison will be for this type of data. We also present computed bifurcation diagrams, that is slices through the solution surface for fixed values of aspect ratio Γ. The two–four exchange process is the simplest, being essentially as described by Schaeffer (1980), and so we present those results first. The four–six exchange is complicated by the presence of non-symmetric solutions, and the bifurcation diagrams are much more complex than those proposed by Benjamin and Schaeffer to explain the experiments.

3.1. *The two–four exchange*

The two-cell primary branch was calculated up to a Reynolds number of 150 at an aspect ratio of 3 using the Keller arclength-continuation method. The Reynolds number was then fixed and the aspect ratio increased up to 4. At this aspect ratio the primary flow has four cells; so, as the Reynolds number is reduced, the two-cell flow, which is now a secondary mode, encounters a limit point. At this point in the experiments the two-cell flow collapses catastrophically and the four-cell flow quickly appears. The two-cell branch at aspect ratio 4 was computed using Keller continuation. Along this branch the Reynolds number decreases until the limit point mentioned above is encountered. This is easy to detect as the Reynolds number begins to increase after the limit point has been passed, though the solution is now unstable, which is indicated by a change in the sign of the determinant of the Jacobian matrix. Once the limit point was found approximately by the above method, the system (2.8) was used to determine its exact location. The entire path of limit points was then calculated using Keller continuation applied to (2.8).

The projection of this path onto the (R, Γ)-plane is shown in figure 1. The region in the small square is shown in magnified form in the inset. This clearly indicates the presence of a non-degenerate hysteresis point, H, and a transcritical bifurcation point, T. This is in agreement with Benjamin's (1978*b*) interpretation of his data. However, whereas Benjamin observed hysteresis for aspect ratios between 3.6 and 3.72, the calculations have hysteresis only between 3.7139 and 3.7154; a very much smaller range. The calculated cusp does point downwards in agreement with the experiments.

We also note that Benjamin's critical Reynolds numbers are, in general, 5–10% lower than those calculated. Cliffe & Mullin (1985) noticed a similar discrepancy in critical Reynolds numbers, for another type of flow, between computed values and those measured in the same apparatus as was used by Benjamin (1978*b*) . They also

† The tables containing these results have been lodged with the *Journal of Fluid Mechanics* editorial office for anyone who wishes to obtain a copy.

pointed out that the outer cylinder, which was made of Perspex tubing, appeared to have become distorted. Thus it seems likely that the quantitative differences between our calculations and Benjamin's experiment are due to the above-mentioned distortions. It should be noted that the calculated hysteresis would be virtually unobservable in an experiment.

Finally in this subsection we present some numerically calculated bifurcation diagrams, that is slices, with Γ fixed, through the solution surface. The radial velocity on the midplane at the gap centre is plotted against Reynolds number for all the solution branches at four different aspect ratios. In figure 3 (*a*) the two-cell flow is the primary flow, as can be seen from the fact that the radial velocity is positive. Figure 3 (*b*) is in the hysteresis region and illustrates the fact that there is virtually no hysteresis. Figure 3 (*c*) is at the aspect ratio that corresponds to the transcritical bifurcation point and again illustrates how close this is to a pitchfork bifurcation point. Finally figure 3 (*d*) shows the four-cell flow as the primary flow. The various solution branches represented in figure 3 were calculated using the Keller arclength method, each branch having about 20 points; the curves were produced using a spline fit to the radial velocity values at the calculated points.

3.2. *The four–six exchange – numerical details*

We expected the four–six exchange to be similar to the two–four exchange described in the previous section. However, it turns out that the situation is complicated by the presence of asymmetric solutions of the Navier–Stokes equations. All these solutions are unstable for the range of aspect ratios we considered and so are not observable, but they do affect the observable flows by reducing the parameter ranges over which they are stable. In the Benjamin–Schaeffer approach to the problem all the flows considered are symmetric and so by implication these authors only allow for symmetric disturbances in their stability analysis. In fact, as we shall demonstrate, the six-cell flow can be unstable to antisymmetric disturbances.

In this subsection we present the numerical details of the calculations for the four–six exchange. The details of the bifurcation structure will be discussed in §3.3. The four-cell primary branch was calculated up to a Reynolds number of 300 at an aspect ratio of 4 using the Keller arclength-continuation method. The radius ratio was fixed at 0.6 to correspond to the data of Mullin (1982). With the Reynolds number fixed at 300 the aspect ratio was increased to 6. At this aspect ratio the primary flow has six-cells and, as in §3.1, when the Reynolds number is reduced a limit point is encountered which marks the lower limiting Reynolds number for the four-cell secondary mode. Once the limit point was located the path of limit points was calculated using Keller continuation applied to (2.8). The projection on the (R, Γ)-plane of this curve is shown in figure 4 as the solid line. The points marked T and H are transcritical bifurcation and non-degenerate hysteresis points respectively.

We located the symmetry-breaking bifurcation on the six-cell secondary branch at aspect ratio 5.0 by computing this flow on the full grid. As R was increased past the bifurcation the determinant of the Jacobian matrix changed sign; we thus located the point approximately. Keller arclength continuation applied to (2.11) was used to compute the path of symmetry-breaking bifurcations, which is indicated by the dashed line in figure 4.

The various degenerate points, H, T, Q, C^+, C^- and D were detected and computed using the techniques described in Cliffe & Spence (1986).

Five bifurcation diagrams shown in figure 5 were computed at values of aspect ratio between 5.0 and 5.6, and these diagrams were obtained by solving the

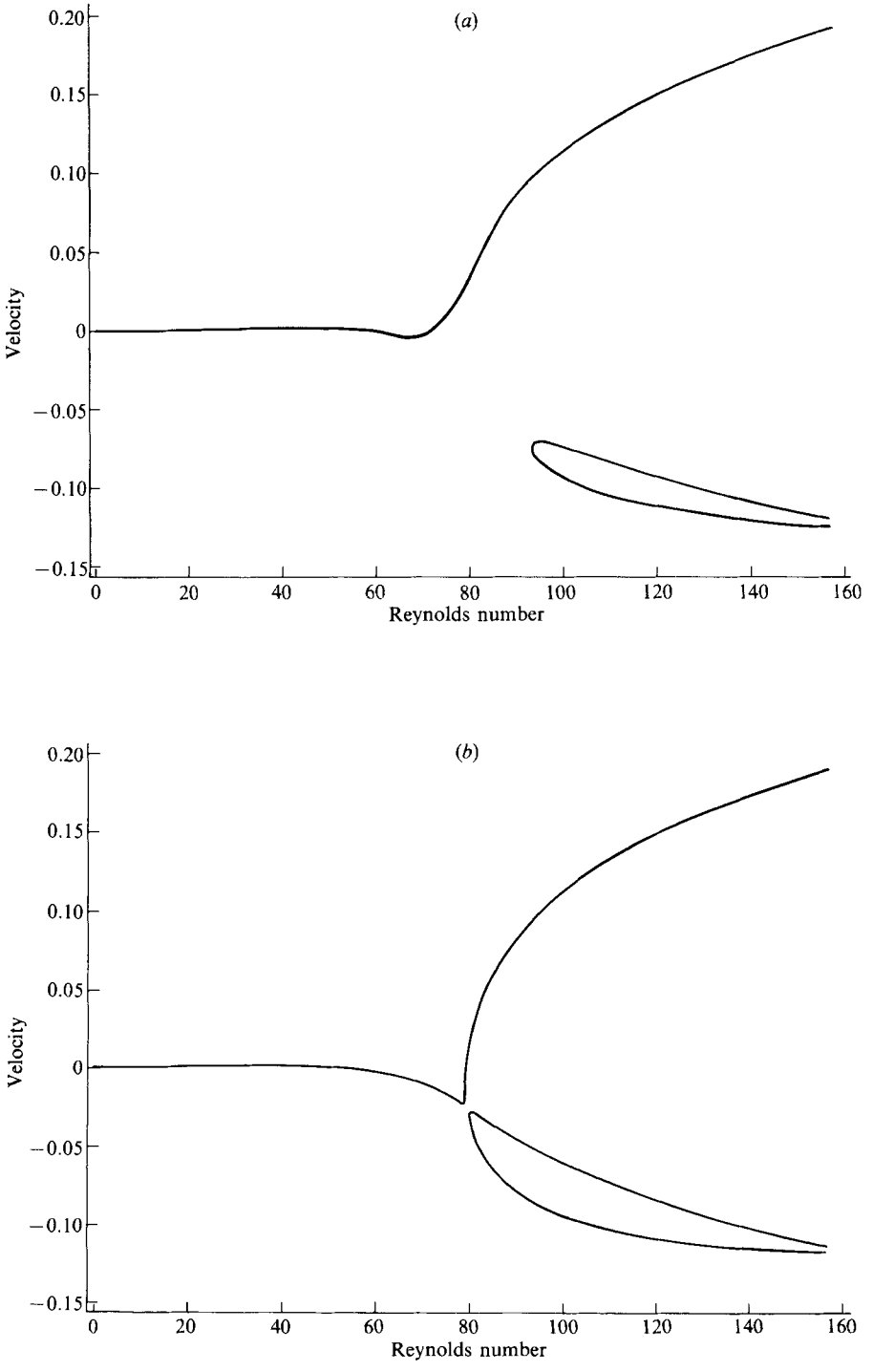

FIGURE 3(*a*, *b*). For caption see facing page.

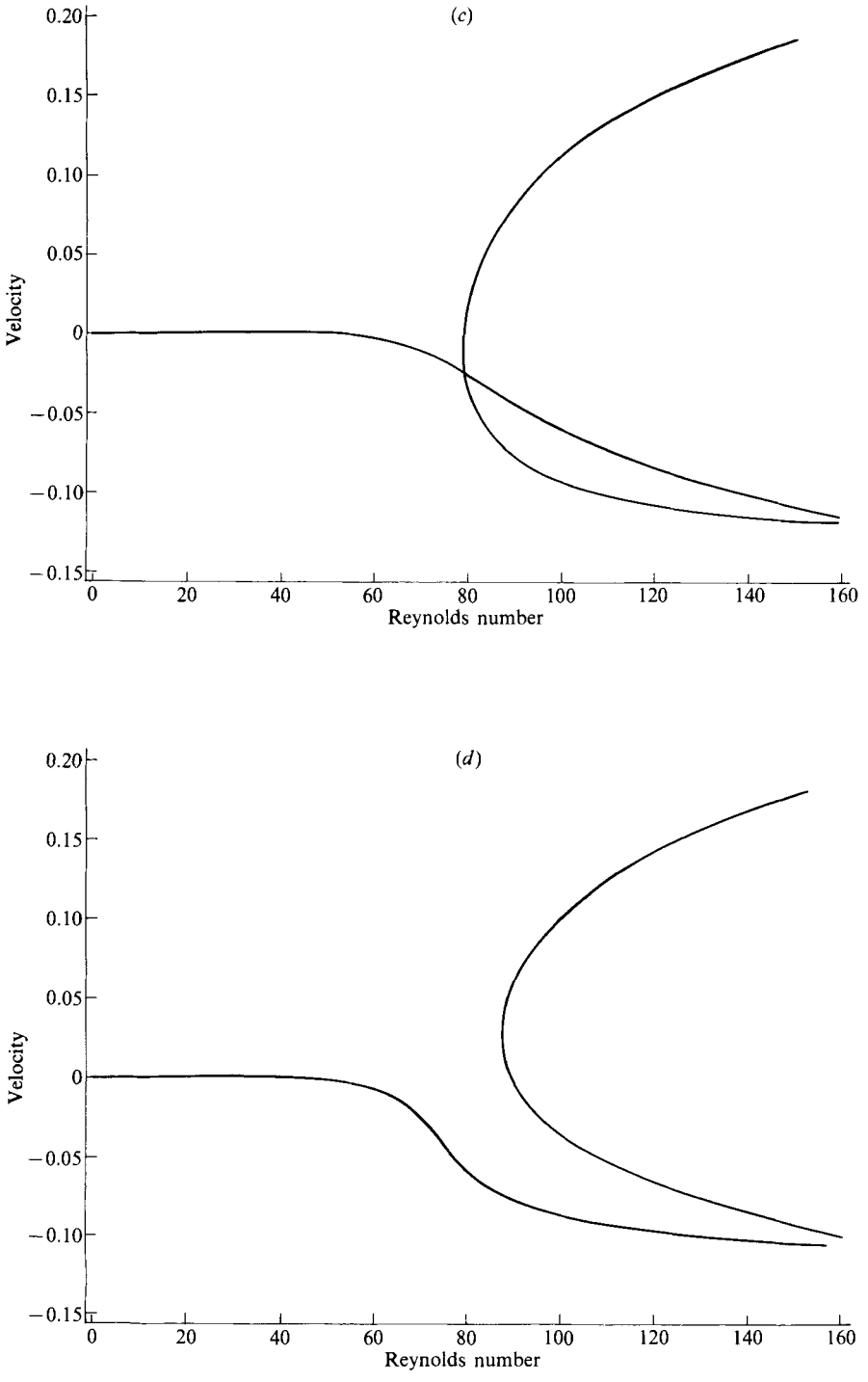

FIGURE 3. Numerically calculated state diagrams for the two–four exchange. The radial component of velocity at the point (0.5, 0) is plotted against Reynolds number for various aspect ratios. (*a*) $\Gamma = 3.6$, (*b*) 3.715, (*c*) 3.71541, (*d*) 4.0.

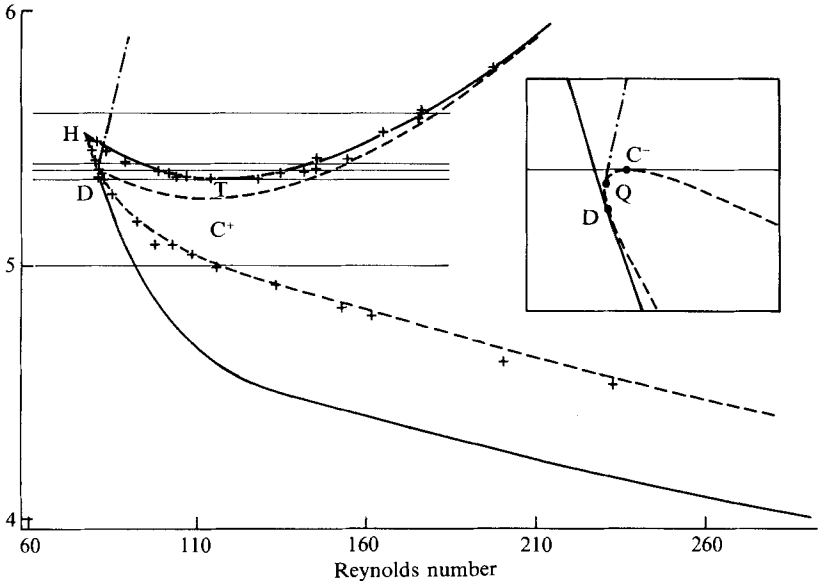

FIGURE 4. Critical loci for four- and six-cell modes with radius ratio 0.6: ——, numerically calculated fold curve; – – – –, numerically calculated path of symmetry-breaking bifurcation points; – · – · –, numerically calculated fold curve for asymmetric solution surface; +, experimental values for four- and six-cell collapse points (from Mullin 1982). An enlargement of the region near the double singular S-point, D, is shown in the inset.

Navier–Stokes equations using Keller arclength continuation. All the solution branches were obtained either as the primary flow starting from zero Reynolds number, or else by branching away from either the path of limit points or the path of symmetry-breaking bifurcation points. For each aspect ratio there are two diagrams which show how the symmetric and antisymmetric parts of the solution behave. The u_r component at $(0.5,0)$ and u_z component at $(0.7,0)$ were taken as the measures of the symmetric and antisymmetric parts of the solution. The asymmetric solutions (i.e. solutions having a non-zero antisymmetric part) are all shown by dashed lines; s denotes a stable and u an unstable part of each curve. In the plots of the antisymmetric component the occurrence of a singularity in the symmetric solution is indicated by a dot. Some care is needed in interpreting the plots of the symmetric component since two solutions may have the same value of $u_r(0.5,0)$ but not coincide. This leads to intersections of the curves that do not correspond to bifurcation points. For example in figure 5(c) the upper dashed line intersects the middle solid line; this is not a bifurcation point as may be seen from examining figure 5(d). Indeed a careful examination of both the symmetric and antisymmetric plots should avoid any such confusion.

The curves shown in the figure were obtained by fitting a cubic spline to the values of the two velocity components computed on a $(5,15,5,S)$ mesh for the symmetric solutions, and a $(5,30,5)$ mesh for the asymmetric solutions. The points themselves are not shown for the sake of clarity, but each diagram is based upon between 100 and 150 points. Incidentally the calculation of these diagrams represents well over half the computational effort required for this problem.

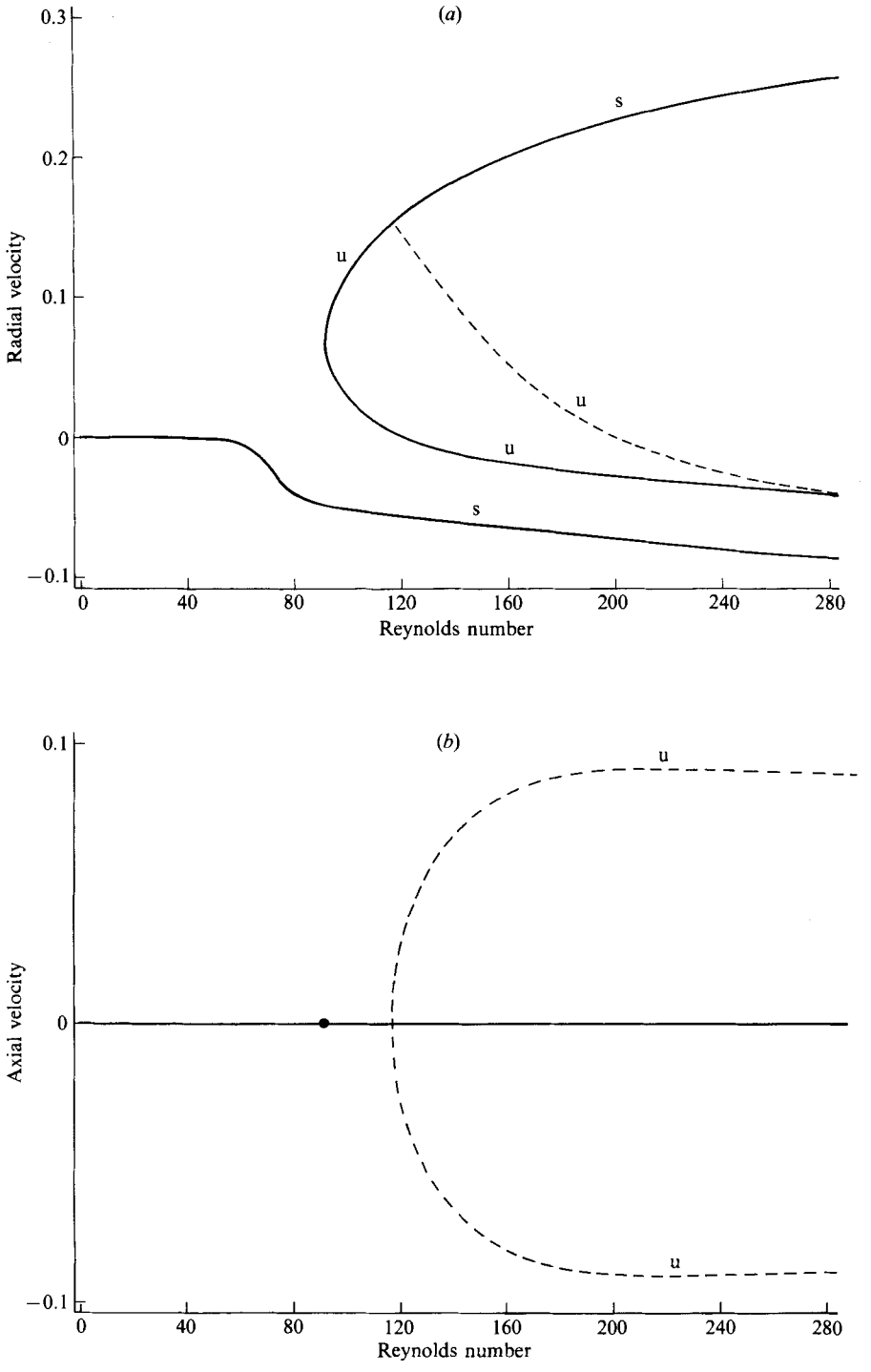

FIGURE 5(*a*, *b*). For caption see p. 73.

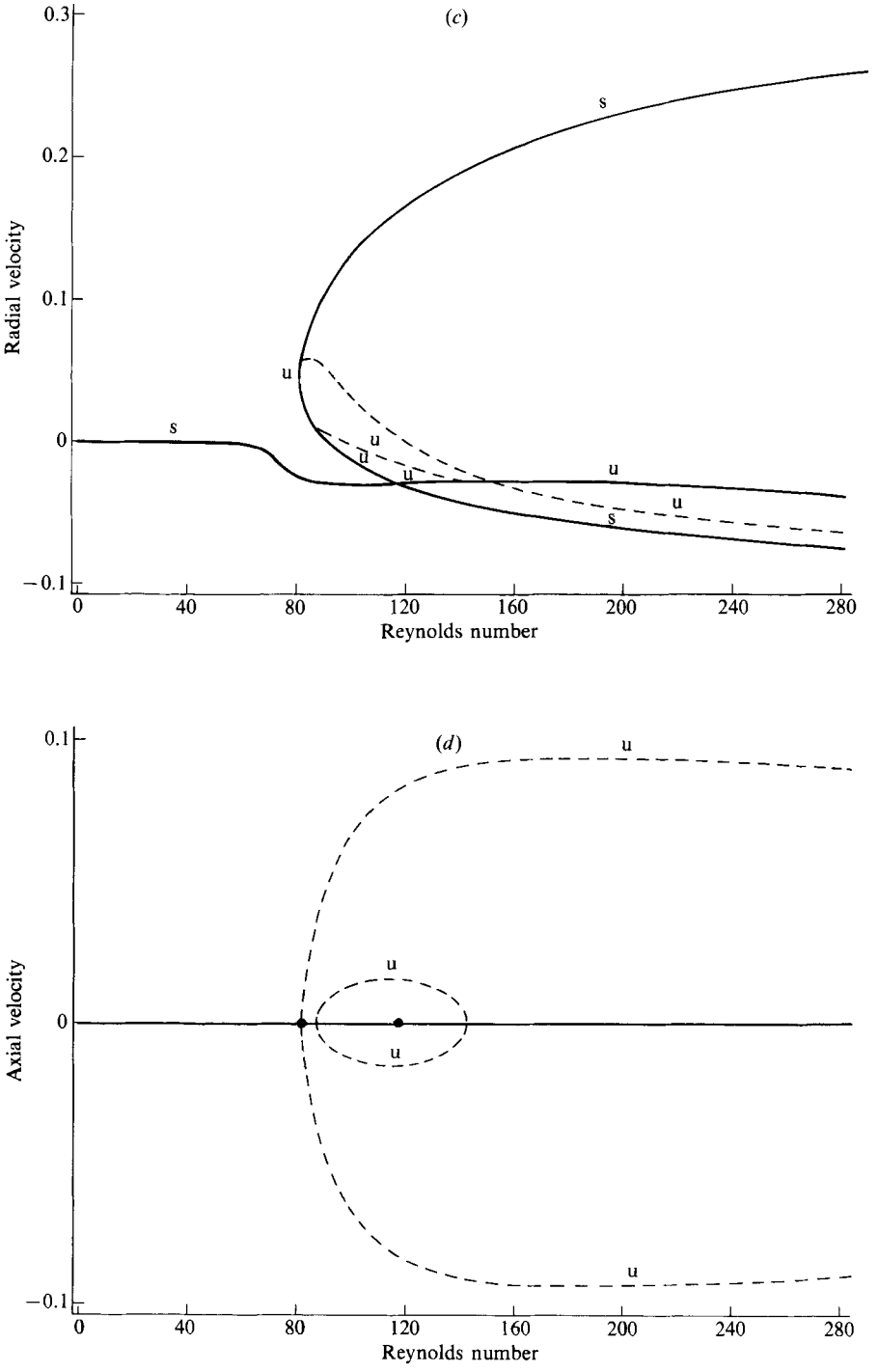

FIGURE 5(*c*, *d*). For caption see p. 73.

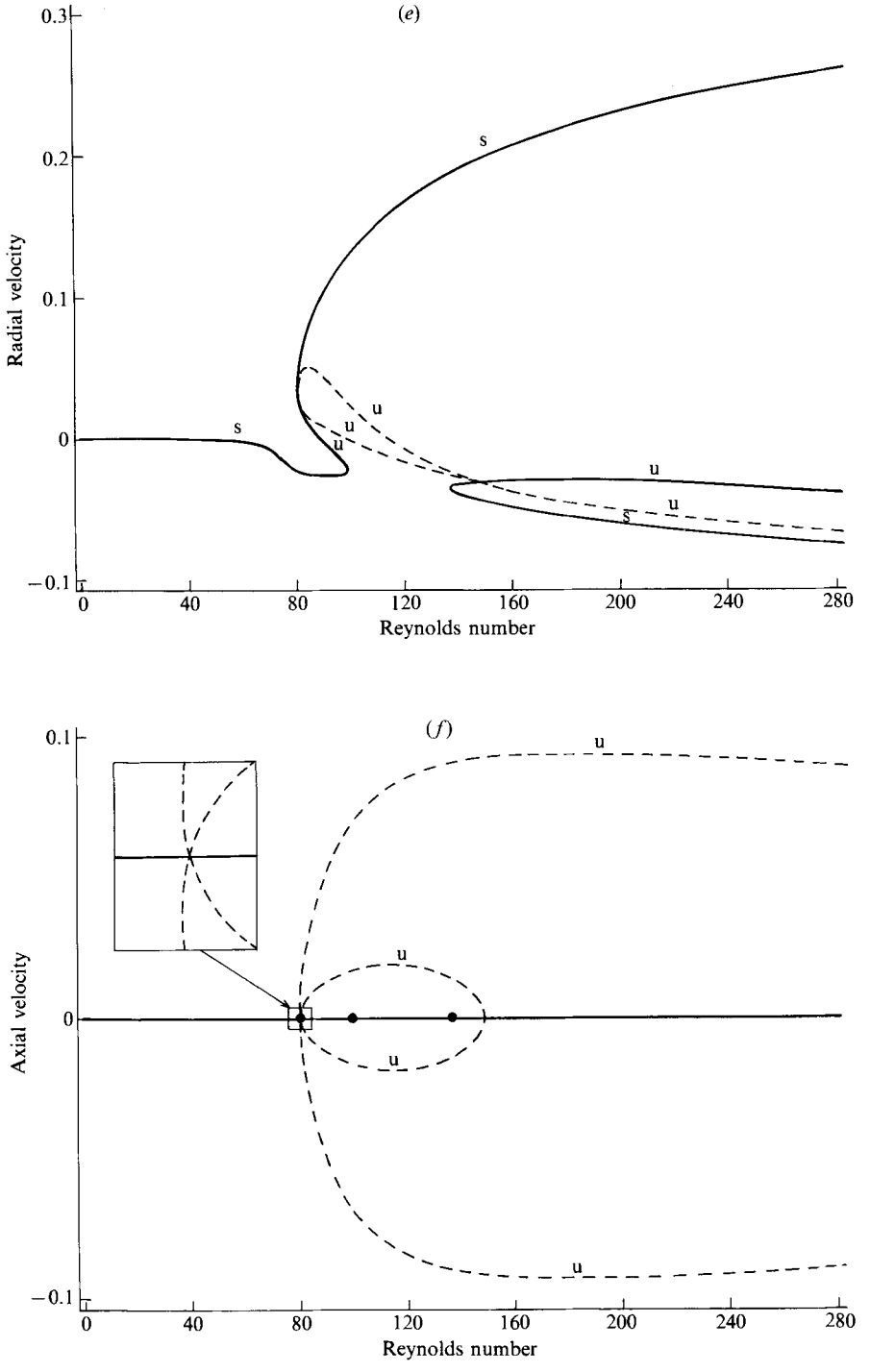

FIGURE 5(*e*,*f*). For caption see p. 73.

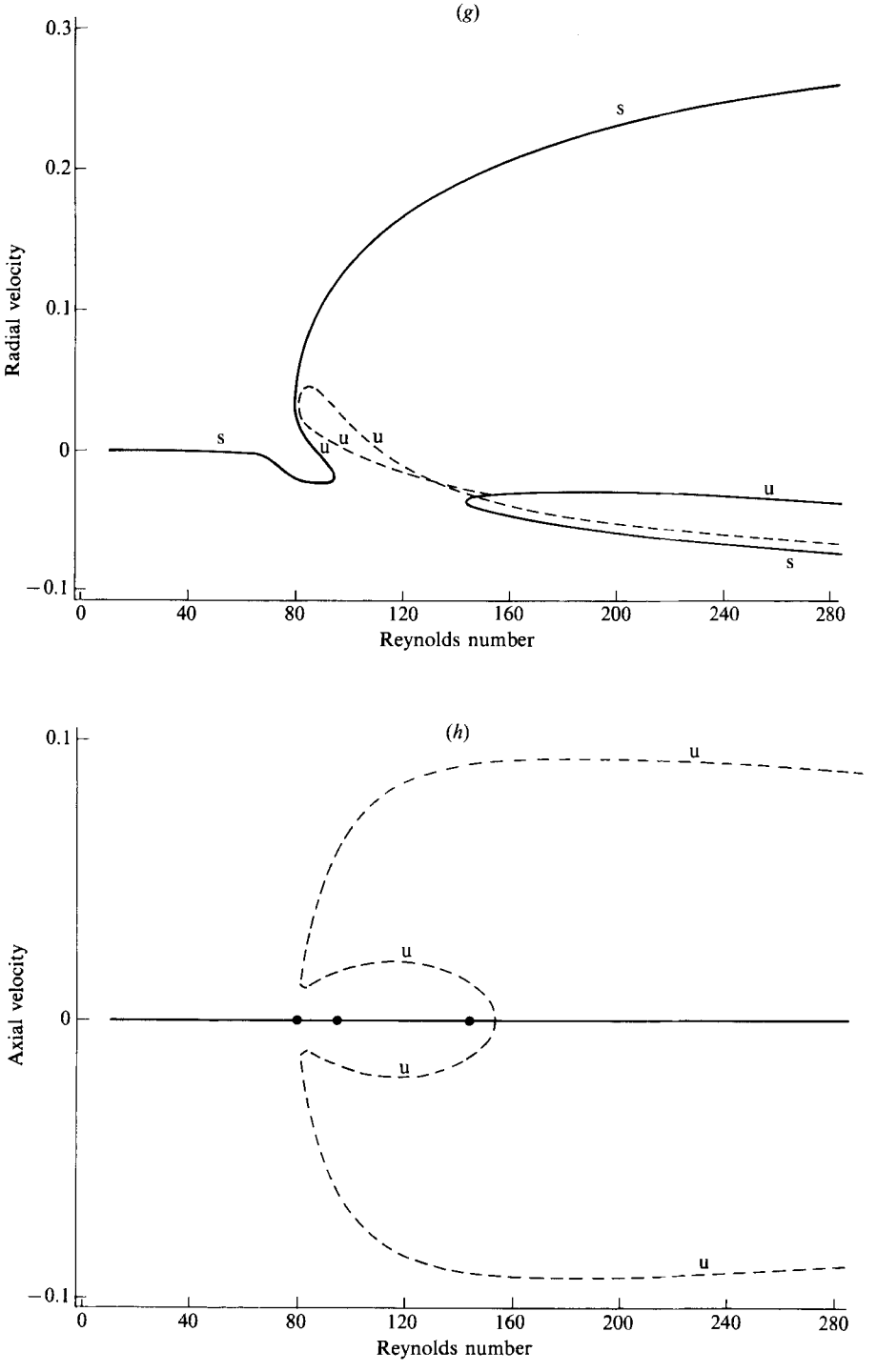

FIGURE 5 (*g*, *h*). For caption see facing page.

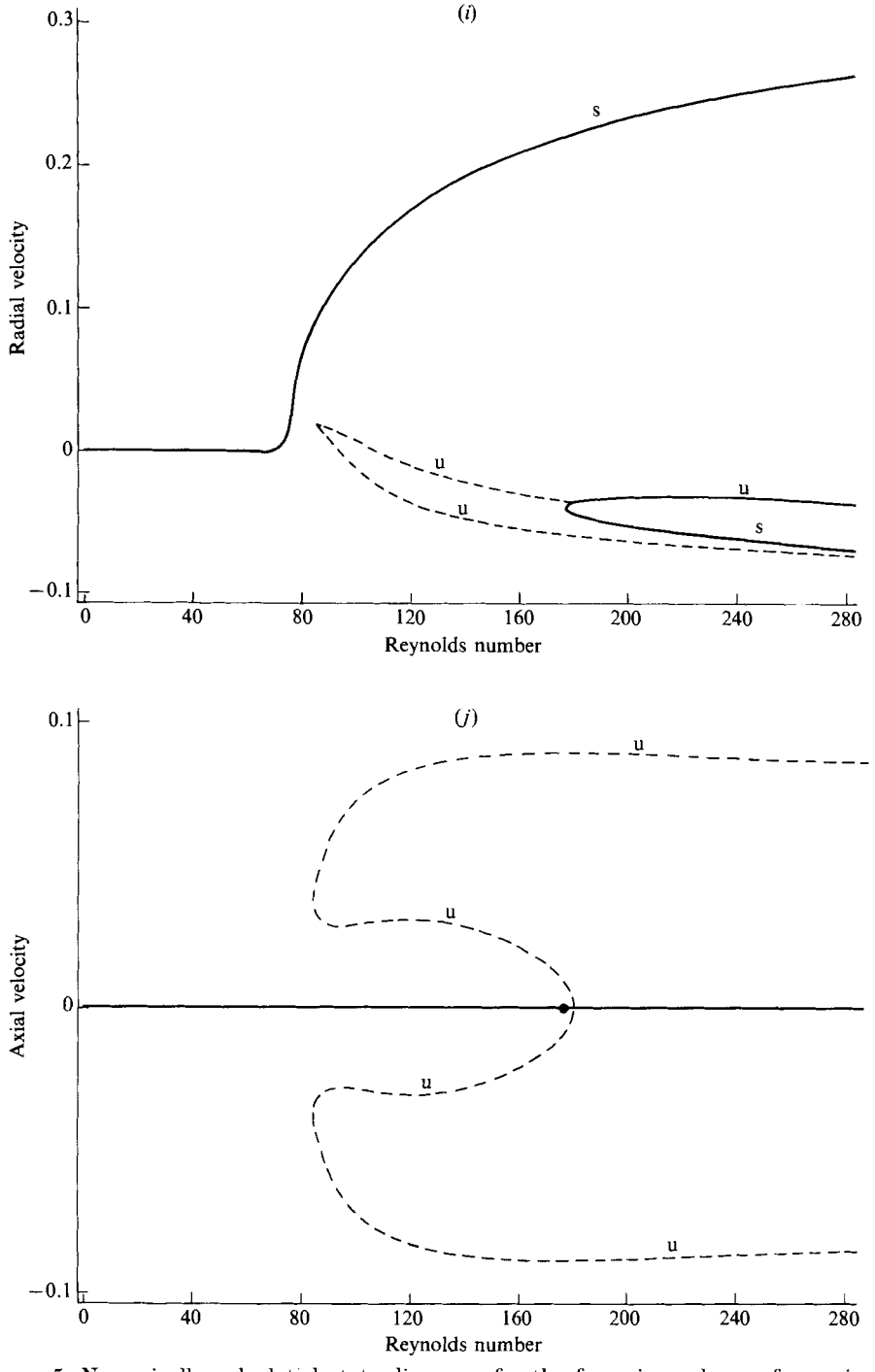

FIGURE 5. Numerically calculated state diagrams for the four–six exchange for various aspect ratios. (a, c, e, g, i) the radial component of velocity at the point (0.5, 0) is plotted against Reynolds number (this measures the symmetric part of the solution). (b, d, f, h, j) the axial component of velocity at the point (0.7, 0) is plotted against Reynolds number (this measures the antisymmetric part of the solution); a solid dot indicates a singularity in the symmetric solution. ——, symmetric solution; – – – –, asymmetric solution. Stable branches are indicated by s and unstable by u. (a, b) $\Gamma = 5.0$, (c, d) 5.3445, (e, f) 5.3798, (g, h) 5.4, (i, j) 5.6.

Similar techniques were used to compute the path of limit points and the path of symmetry-breaking bifurcations for a radius ratio of 0.507 which corresponds to the experiment of Mullin *et al.* (1982). The results are shown in figure 8.

3.3. *The four–six exchange - bifurcation structure*

In this subsection we discuss in detail the bifurcation structure associated with the four–six exchange and its relationship to the experimental observations of Mullin (1982). The situation is complicated by the presence of symmetry-breaking bifurcations. In order to make the presentation as clear as possible we shall discuss the symmetric flows first. We shall use the notation $\Gamma(X)$ $(R(X))$ to denote the aspect ratio (Reynolds number) at the point X in figure 4, where X is one of H, T, Q, C^+, C^-, D.

The computed path of limit points of the symmetric solution is shown in figure 4. For aspect ratio less than Γ(T) the bifurcation diagram looks like figure 5(*a*) (ignoring for the moment the dashed line). The four-cell primary flow develops smoothly as R is increased from zero and there is a branch of six-cell flows for sufficiently large R. The lower stability limit of the six-cell flow is determined by the limit point. As the aspect ratio is increased the four-cell branch and the lower part of the six-cell branch approach each other until, at aspect ratio Γ(T), they touch, giving rise to the transcritical bifurcation shown in figure 5(*c*). The situation for slightly larger aspect ratio is shown in figure 5(*e*). Here the primary branch first develops a weak four-cell structure until a limit point is encountered. At this point the weak four-cell flow collapses and a six-cell flow is formed. Thus in the aspect-ratio range between Γ(T) and Γ(H) hysteresis phenomena are observable. Figure 5(*e*) also shows that the four-cell flow is a secondary mode in this region. Streamline plots of the four- and six-cell flows in this hysteresis region are shown in figure 6. As the aspect ratio is increased further the two limit points on the six-cell branch approach each other and finally coalesce at the nondegenerate hysteresis point H. For larger aspect ratios the primary flow has six cells and the bifurcation diagram looks like figure 5(*i*).

This sequence of events is precisely the same as Schaeffer (1980) obtained from his analysis. It is also consistent with the work of Hall, (1982) in that the cusp points upwards; however, Hall's analysis gave a much smaller region of hysteresis than our numerical calculations. This is not particularly surprising since he was applying a perturbation method with the small parameter probably outside the region of validity for the method. In figure 4 we have also shown Mullin's (1982) experimental data. For the part of the path of limit points above the point marked D the agreement between the data and the numerical calculations is very good; however, for aspect ratios less than Γ(D) there is a considerable deviation. The reason for this is that for values of aspect ratio less than Γ(D) the six-cell secondary mode loses stability, owing to antisymmetric disturbances, at Reynolds numbers greater than those corresponding to the limit point. The situation is illustrated in figures 5(*a*) and 5(*b*) for aspect ratio 5.0. For Reynolds numbers greater than 118 the upper part of the six-cell branch is stable. At a Reynolds number of 118 there is a supercritical symmetry-breaking bifurcation and a pair of unstable asymmetric solutions (dashed lines) branch away from the symmetric solution. The six-cell flow is unstable for Reynolds numbers less than 118 and so collapses to a four-cell flow. Thus for aspect ratios below Γ(D), Mullin's experimental measurements of the stability limit of the six-cell flow correspond to symmetry-breaking bifurcation points. This path of computed symmetry-breaking bifurcations is shown by the dashed line in figure 4

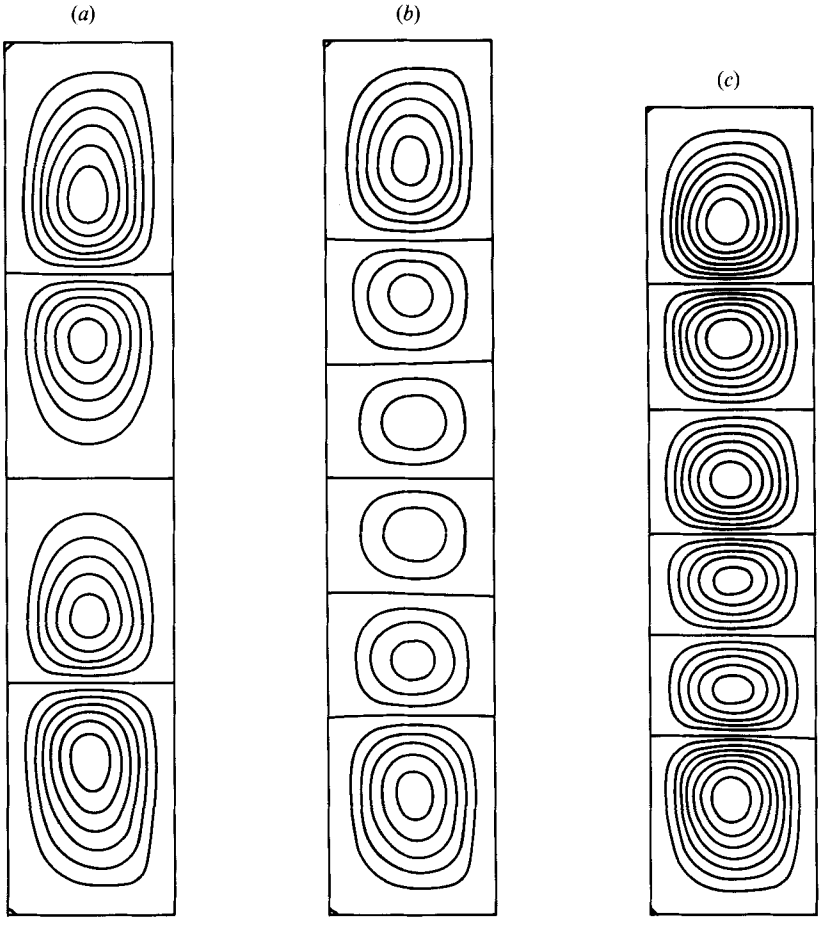

FIGURE 6. Streamline plots with inner cylinder on right: (*a*) stable four-cell flow at aspect ratio 5.4 and Reynolds number 94.1; (*b*) stable six-cell flow at aspect ratio 5.4 and Reynolds number 81.9; (*c*) asymmetric six-cell flow at aspect ratio 5.0 and Reynolds number 129.9.

and it can be seen that the agreement between calculation and experiment is good.

Thus the computed stability limits of the four- and six-cell flows in this problem agree rather well with the experimental data of Mullin (1982). It is also interesting to note that the problem appears to be somewhat more complex than Schaeffer's analysis would indicate in that asymmetric modes play a role in the exchange process, albeit an indirect one since they are all unstable.

We turn now to the asymmetric solutions. The presence of symmetry breaking and the resulting asymmetric solutions lead to an unexpectedly complex solution set. We shall discuss the bifurcation structure implied by figure 4 by making use of the bifurcation diagrams in figure 5, and describe how the bifurcation picture changes as the aspect ratio increases from 5.0 to 5.6. For aspect ratios less than $\Gamma(C^+)$ the picture is relatively straightforward; a pair of unstable asymmetric six-cell flows branch away supercritically from the upper part of the six-cell branch (see figures 5*a* and 5*b*). This pair of solution branches exists for increasing R and has no bifurcation points or singularities (at least up to $R = 280$ where our calculations stop). A

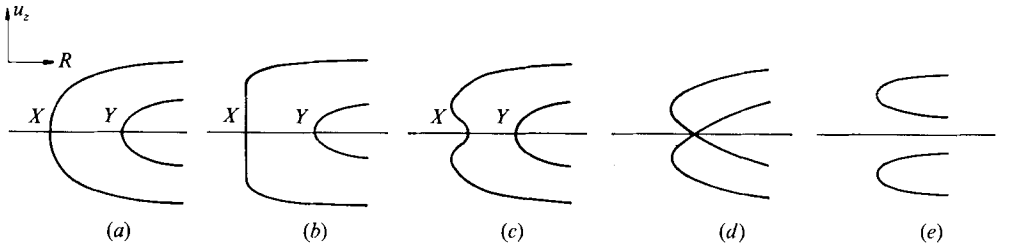

FIGURE 7. A schematic plot of a measure of the antisymmetric component of the solution against R in the region near D, Q and C^- (cf. figure 4). (*a*) $\Gamma(D) > \Gamma > \Gamma(Q)$, (*b*) $\Gamma = \Gamma(Q)$, (*c*) $\Gamma(Q) < \Gamma < \Gamma(C^-)$, (*d*) $\Gamma = \Gamma(C^-)$, (*e*) $\Gamma > \Gamma(C^-)$.

streamline plot of this unstable asymmetric six-cell flow is shown in figure 6(*c*) (the aspect ratio is 5.0 and R is about 10% above the bifurcation value). The two cells just below the midplane are slightly smaller than those above it. The two branches are mirror images of each other so that the other branch would have the smaller cells above the midplane.

At an aspect ratio of $\Gamma(C^+)$ a loop of asymmetric solutions is formed on the lower (unstable) part of the six-cell solution branch. This loop can be clearly seen in figure 5(*d*). As the aspect ratio is reduced towards $\Gamma(C^+)$ the two symmetry-breaking bifurcations at the extremes of the loop approach each other and eventually coalesce at C^+.

The next significant event occurs when the aspect ratio reaches $\Gamma(T)$ where the four-cell branch touches the lower part of the six-cell branch producing the transcritical bifurcation in figure 5(*c*). Note that the four-cell branch touches the six-cell branch at a point lying between the two extremes of the asymmetric loop that formed at C^+. This can be seen from figure 5(*d*) where the solid dot at Reynolds number ~ 118 indicates the transcritical bifurcation point. The solid dot at Reynolds number ~ 81 indicates the limit point on the six-cell solution branch. The symmetry-breaking bifurcation point on the upper part of the six-cell branch is clearly very close to this limit point and as the aspect ratio is increased to $\Gamma(D)$ the two points coincide. Beyond $\Gamma(D)$ the symmetry-breaking bifurcation is still supercritical but now lies on the middle part of the primary branch which is, of course, S-shaped in the region between $\Gamma(T)$ and $\Gamma(H)$.

In the region between $\Gamma(D)$ and $\Gamma(C^-)$ this symmetry-breaking bifurcation interacts with that at the low-Reynolds-number extreme of the asymmetric loop formed at C^+. This region is shown in enlarged form in the inset of figure 4. Figure 7 shows, in schematic form, the antisymmetric part of the bifurcation diagram in this region. (This is the relevant part as the symmetric solution structure does not change.) The bifurcation at X in figure 7 corresponds to points on the path between D and C^- and that at Y to points at Reynolds numbers greater than $R(C^-)$. As the aspect ratio increases through $\Gamma(Q)$ the bifurcation X changes from being supercritical to being subcritical. At Q the bifurcating branches depend on the fourth power of the excess Reynolds number. For aspect ratios greater than $\Gamma(Q)$ each asymmetric branch has a limit point, as shown in figure 7(*c*). These paths are indicated in figure 4 by the chain dotted line. There is only one line since the limit points on the two branches have the same critical Reynolds number (by the symmetry of the problem). As the aspect ratio is increased to $\Gamma(C^-)$ the bifurcations at X and Y get closer together and coalesce at C^-, as shown in figure 7(*d*). The

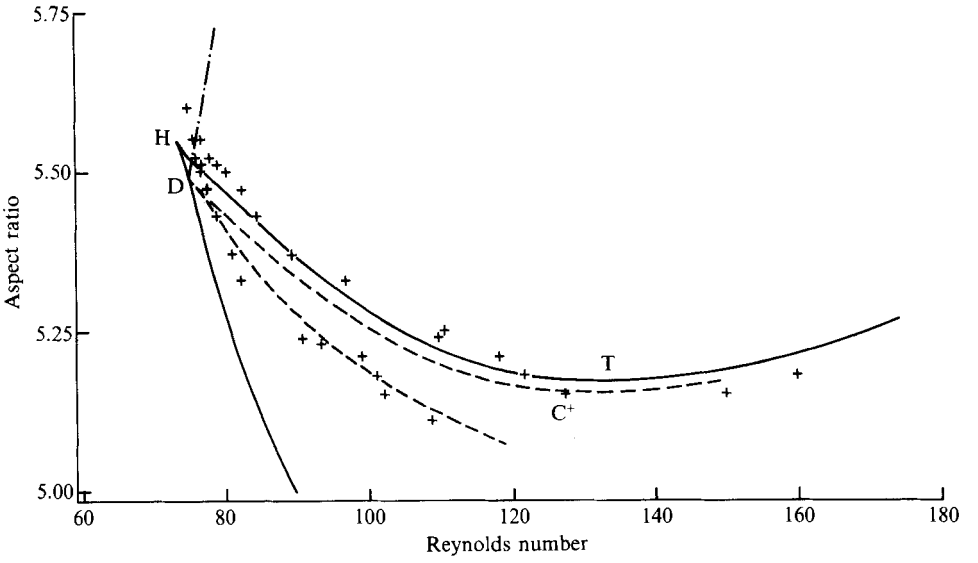

FIGURE 8. As for figure 4 but with radius ratio 0.507 and experimental points from Mullin *et al.* (1982).

complete, computed, bifurcation diagram at $\Gamma(C^-)$ is given in figures 5(*e*) and 5(*f*). As the aspect ratio increases beyond $\Gamma(C^-)$ the asymmetric solutions separate from the middle part of the S-shaped primary solution branch (figures 5*g*, 5*h* and 7*e*).

Thus for aspect ratios greater than $\Gamma(C^-)$ the asymmetric solutions bifurcate subcritically from the symmetry-breaking bifurcation on the upper part of the four-cell branch. At lower values of the Reynolds number there is a limit point on each of these branches which then move off in the direction of increasing R as shown in figure 5(*g–j*).

Finally we remark that a similar set of results was obtained at a radius ratio of 0.507 which corresponds to the experiment of Mullin *et al.* (1982). The computed and experimental results are shown in figure 8 where there is a similar level of agreement to that in figure 4 bearing in mind the fact that figure 8 covers a much smaller range of aspect ratios.

4. Conclusions

We have applied various methods for solving nonlinear equations and bifurcation problems to a finite-element discretization of the steady axisymmetric Navier–Stokes equations with boundary conditions appropriate to the Taylor problem with the outer cylinder and the ends of the annulus stationary. We have considered the problem of the way in which the number of cells present in the primary flow changes as the length of the annulus varies. The results for the exchange between a two-cell and four-cell flow are in qualitative agreement with the experimental data of Benjamin and support his interpretation of the phenomenon. However, there are certain quantitative differences, the most notable being the very small range of aspect ratios over which hysteresis was present in the calculations compared with that observed by Benjamin. The reason for this discrepancy is not obvious. The qualitative theory developed by Schaeffer (1980) would appear to give the right type

of behaviour of this case in spite of the fact that his model is only strictly applicable to the cases with more than two cells present.

The situation with regard to the four–six exchange is more interesting in that for a certain range of aspect ratios the six-cell secondary mode loses stability to antisymmetric disturbances. This possibility was not treated by Schaeffer, who assumed that all the flows were symmetric. The presence of asymmetric solutions in the exchange process gives rise to a rich solution structure which we feel is interesting in its own right. There is good quantitative agreement between the experimental data of Mullin (1982) and Mullin *et al.* (1982) and the calculations for the limits of stability of the four- and six-cell flows.

The author is grateful to Dr T. Mullin for providing the experimental data used in figures 4 and 8 in tabulated form and to him and the referees for helpful comments on the first version of this paper. This work was undertaken as part of the Underlying Research Programme of the UKAEA.

REFERENCES

Benjamin, T. B. 1978*a* Bifurcation phenomena in steady flows of a viscous liquid. I. Theory. *Proc. R. Soc. Lond.* A **359**, 1–26.

Benjamin, T. B. 1978*b* Bifurcation phenomena in steady flows of a viscous liquid. II. Experiments. *Proc. R. Soc. Lond.* A **359**, 27–43.

Benjamin, T. B. & Mullin, T. 1982 Notes on the multiplicity of flows in the Taylor experiment. *J. Fluid Mech.* **121**, 219–230.

Cliffe, K. A. 1983 Numerical calculations of two-cell and single-cell Taylor flows. *J. Fluid Mech.* **135**, 219–233.

Cliffe, K. A., Jackson, C. P. & Greenfield, A. C. 1982 Finite-element solutions for flow in a symmetric channel with a smooth expansion. *Harwell Rep.* AERE R-10608. HMSO.

Cliffe, K. A., Jepson, A. & Spence, A. 1986 The numerical solution of bifurcation problems with symmetry with application to the finite Taylor problem. In *Numerical Methods for Fluid Dynamics II* (ed. K. W. Morton & M. J. Baines), pp. 155–176. Clarendon.

Cliffe, K. A. & Mullin, T. 1985 A numerical and experimental study of anomalous modes in the Taylor experiment. *J. Fluid Mech.* **153**, 243–258.

Cliffe, K. A. & Spence, A. 1984 The calculation of high order singularities in the finite Taylor problem. In *Numerical Methods for Bifurcation Problems* (ed. T. Küpper, H. D. Mittelmann & H. Weber), pp. 129–144. Birkhäuser: ISNM.

Cliffe, K. A. & Spence, A. 1986 Numerical calculations of bifurcations in the finite Taylor problem. In *Numerical Methods for Fluid Dynamics II* (ed. K. W. Morton & M. J. Baines), pp. 177–197. Clarendon.

Engleman, M. S., Sani, R. L., Gresho, P. M. & Bercovier, M. 1982 Consistent vs. reduced integration penalty methods for incompressible media using several old and new elements. *Intl J. Num. Meth. Fluids* **2**, 25–42.

Golubitsky, M. & Schaeffer, D. G. 1979 A theory of imperfect bifurcation via singularity theory. *Communs Pure Appl. Maths* **32**, 21–98.

Hall, P. 1980 Centrifugal instabilities in finite containers: a periodic model. *J. Fluid Mech.* **99**, 575–596.

Hall, P. 1982 Centrifugal instabilities of circumferential flows in finite cylinders: the wide gap problem. *Proc. R. Soc. Lond.* A **384**, 359–379.

Jepson, A. & Spence, A. 1985 Folds in solutions of two parameter systems. *SIAM J. Numer. Anal.* **22**, 347–368.

Keller, H. B. 1977 Numerical solutions of bifurcation and nonlinear eigenvalue problems. In *Applications of Bifurcation Theory* (ed. P. H. Rabinowitz), pp. 359–384. Academic.

KUSNETSOV, E. A., LVOV, V. S., NESTERIKHIN, Y. E., SHMOJLOV, Y. F., SOBOLEV, V. S., SPECTOR, M. D., TIMOKHIN, S. A., UTKIN, E. N. & VASILENKO, Y. G. 1977 About turbulence arising in Couette flows. *Inst. Automation and Electrometry, Siberian Branch, USSR Acad. Sci., Preprint no.* 58.

MOORE, G. & SPENCE, A. 1980 The calculation of turning points of nonlinear equations. *SIAM J. Numer. Anal.* **17**, 567–576.

MULLIN, T. 1982 Mutations of steady cellular flows in the Taylor experiment. *J. Fluid Mech.* **121**, 207–218.

MULLIN, T., PFISTER, G. & LORENZEN, A. 1982 New observations on hysteresis effects in Taylor–Couette flow. *Phys. Fluids* **25**, 1134–1136.

ROBERTS, P. H. 1965 Appendix to Experiments on the stability of viscous flow between rotating cylinders. VI. Finite amplitude experiments. *Proc. R. Soc. Lond.* A **283**, 531–533.

SCHAEFFER, D. G. 1980 Analysis of a model in the Taylor problem. *Math. Proc. Camb. Phil. Soc.* **87**, 307–337.

SCHRAUF, G. 1986 The first instability in spherical Taylor–Couette flow. *J. Fluid Mech.* **166**, 287–303.

TUCKERMAN, L. S. 1983 Formation of Taylor vortices in spherical Couette flow. Ph.D. thesis, Massachusetts Institute of Technology.

WERNER, B. 1984 Regular systems for bifurcation points with underlying symmetries. In *Numerical Methods for Bifurcation Problems* (ed. T. Küpper, H. D. Mittelmann & H. Weber), pp. 562–574. Birkhäuser: ISNM.

WERNER, B. & SPENCE, A. 1984 The computation of symmetry-breaking bifurcation points. *SIAM J. Numer. Anal.* **21**, 388–399.